The 2025 World Congress on
Advances in Structural Engineering and Mechanics (ASEM25)
BEXCO, Busan, Korea, August 11-14, 2025

Optimal Design and Performance Evaluation of Novel TMDI Configurations for Seismic Vibration Mitigation

*Lili Zhou[1), 3)], Yung-Tsang Chen[1), 2)], Jing Bie[1), 4)], Byung Gyoo Kang[1), 4)]

[1), 2)] Department of Civil Engineering , University of Nottingham Ningbo China, Ningbo 315100, China
[3)] Faculty of Architecture and Art , Ningbo Polytechnic University, Ningbo 315800, China
[2)] Yung-Tsang.Chen@nottingham.edu.cn

ABSTRACT

This study introduces two innovative floor-connected tuned mass damper inerter (TMDI) configurations, achieved through a strategic reconfiguration of damper-inerter connections. Utilizing analytical methods and fixed-point theory, closed-form solutions for the optimal frequency and damping ratios in single-degree-of-freedom systems are derived. A comparative analysis under white noise excitation establishes a performance hierarchy: the grounded TMDI outperforms the conventional TMD, which in turn surpasses the series floor-connected TMDI (TMDI-II), with the parallel floor-connected TMDI (TMDI-I) exhibiting the lowest performance. Parametric studies highlight that the placement of the inerter significantly influences vibration mitigation efficiency, with grounded configurations demonstrating superior performance compared to their floor-connected counterparts. The optimality criteria and configuration comparisons derived offer critical insights for the design of seismic protection systems, particularly in mass-sensitive structures.

KEYWORDS
Tuned mass damper inerter (TMDI), seismic vibration mitigation, optimal design, parametric study, closed-form solutions

1. INTRODUCTION

Structural vibration control remains a paramount concern in civil engineering, particularly for structures subjected to dynamic loads such as earthquakes excitations. Traditional seismic vibration mitigation strategies, including tuned mass dampers (TMDs), have been widely adopted but face inherent limitations due to their mass-

---

[1)] Graduate Student
[2)] Associate Professor
[4)] Assistant Professor

dependent performance and sensitivity to frequency detuning (Lazar et al., 2014; Pietrosanti et al., 2017; Smith, 2002). To address these challenges, the tuned mass damper inerter (TMDI) system has emerged as a promising advancement, integrating the inertial amplification mechanism of the inerter—a two-terminal mechanical device generating force proportional to relative acceleration—to achieve superior vibration attenuation with reduced mass requirements (Giaralis and Taflanidis, 2018; Khorsand and Rofooei, 2024).

The TMDI concept builds upon the classical TMD framework while introducing critical enhancements. Early studies by Smith (2002) demonstrated the ability of the inerter to amplify apparent mass, enabling effective energy dissipation without proportional physical mass addition. Subsequent research by Lazar et al. (2014) validated this principle through analytical and experimental studies, showing that TMDI configurations could suppress vibrations 40–60% more effectively than conventional TMDs under harmonic excitations. These findings were further extended by Pietrosanti et al. (2020), who developed a generalized two-degree-of-freedom model to optimize TMDI performance in multi-degree-of-freedom (MDOF) structures, highlighting improved dynamic response control through inertial amplification.

Despite these advancements, practical deployment of TMDI systems requires addressing several critical challenges: (1) the configuration adaptability to complex structural geometries remains underexplored, particularly for irregular high-rise buildings where mode shapes and frequency distributions vary significantly across heights (Zhang, et al., 2023), (2) the frequency uncertainty—stemming from material aging, construction variability, and soil-structure interaction—poses persistent challenges to optimal tuning (Ruiz, R. et al., 2018). Additionally, the frequency uncertainty of earthquake loads also presents a challenge to the performance of TMDI systems (Giaralis and Petrini, 2017). This uncertainty may result in TMDI systems failing to achieve the expected vibration control effects in practical applications. Therefore, this factor must be fully considered during system design. (3) Multi-objective optimization of TMDI parameters (mass ratio, inertance ratio, damping coefficients) demands rigorous analytical frameworks to balance conflicting performance criteria such as displacement reduction, acceleration mitigation, and economic feasibility (Giaralis and Taflanidis, 2018; Li, 2022).

Recent studies have explored innovative TMDI configurations to overcome these limitations. Giaralis and Taflanidis (2018) proposed a reliability-based design framework for MDOF structures, incorporating model uncertainties and using white noise excitation to evaluate stochastic responses. Lara-Valencia et al (2020) introduced an exhaustive search optimization method, minimizing peak structural displacements and root-mean-square accelerations through systematic parameter calibration. For nonlinear systems, Khorsand and Rofooei (2024) assessed TMDI performance under near-fault and far-field earthquake records, revealing significant reductions in story drifts and residual deformations when combined with auxiliary damping systems.

Existing TMDI systems predominantly adopt a "grounded" configuration, where one end of the inerter connects to the main structure and the other anchors to the ground. This design introduces two critical issues: (1) the complexity of underground anchor construction increases maintenance costs by 35% (De Domenico et al., 2018); and (2) phase differences between ground motion inputs and structural responses

reduce the acceleration differential across the inerter, constraining its virtual mass effect (Marian and Giaralis, 2014). To address these challenges, recent studies have explored innovative TMDI configurations that deviate from the traditional grounded design. For instance, some researchers have proposed floating or semi-active TMDI systems that do not require a direct connection to the ground, thereby reducing maintenance costs and eliminating the phase difference issue (Ruiz et al., 2018; Sun and Tong, 2024). Other studies have focused on optimizing the parameters of the TMDI system, such as the mass ratio, inertance ratio, and damping coefficients, to achieve a balance between performance and economic feasibility (Petrini et al., 2020).

In addition, research into the application of TMDI systems in various engineering fields has expanded. For example, in bridge engineering, TMDI systems have been investigated for their potential to mitigate vortex-induced vibrations in long-span bridges (Dai et al., 2021). Vortex-induced vibrations, caused by wind flowing around bridge decks, can lead to significant fatigue damage and reduce the service life of bridge components. TMDI systems offer a promising solution for mitigating these vibrations and enhancing the structural integrity of long-span bridges. In wind energy, TMDI systems have been explored for their ability to enhance the stability of wind turbines and improve energy harvesting efficiency (Zhang and Fitzgerald, 2020). By mitigating vibrations in wind turbine blades and towers, TMDI systems can contribute to the reliable and efficient operation of wind turbines, thereby increasing energy production and reducing maintenance costs.

Furthermore, advancements in materials science and smart technologies have opened up new possibilities for TMDI design. The integration of shape memory alloys, magnetorheological elastomers, and other smart materials into TMDI systems has enabled the development of adaptive and semi-active control strategies (Sun and Tong, 2024). In particular, the application of shape memory alloys offers new possibilities for the development of adaptive TMDI systems (Song et al., 2006). By utilizing the temperature-dependent phase transformation characteristics of shape memory alloys, real-time regulation of the dynamic characteristics of TMDI systems can be achieved, thereby further enhancing the system's vibration control performance. These smart materials offer the unique capability to change their mechanical properties in response to external stimuli, such as temperature, electric fields, or magnetic fields. By incorporating these materials into TMDI systems, it is possible to create adaptive dampers that can adjust their damping characteristics in real-time to match the changing dynamic conditions of the host structure (Petrini et al., 2020; Ruiz et al., 2018). These strategies offer the potential for improved performance and robustness under varying environmental conditions, making TMDI systems even more versatile and effective.

In conclusion, while the grounded configuration of TMDI systems has been widely adopted, it is not without its drawbacks. The increased maintenance costs and phase difference issue highlight the need for continued research and development of alternative TMDI configurations and optimization strategies. The exploration of new TMDI systems, the optimization of system parameters, and the integration of smart materials represent promising avenues for advancing the state-of-the-art in TMDI technology.

This study contributes to the growing body of TMDI research by introducing two

novel floor-connected TMDI configurations and conducting comprehensive performance evaluations. Unlike conventional grounded TMDI systems, the proposed configurations strategically reconfigure damper-inerter connections. The subsequent sections are organized as follows: Section 2 develops the analytical model for the main structure with proposed TMDI configurations, incorporating parameter variations. Section 3 presents frequency domain analysis through displacement transfer functions and time domain validation via white noise excitation simulations. The concluding section summarizes key findings and proposes recommendations for practical implementation of TMDI technology in building structures.

2. Modelling

2.1 Main Structure

The main structure is modeled as a single-degree-of-freedom (SDOF) system representing the critical vibration mode to be mitigated by the damper. The governing equation of motion is given by:

$$m_s\ddot{u}_s(t) + c_s\dot{u}_s(t) + k_s u_s(t) = f(t) \tag{1}$$

$$c_s = 2m_s\omega_s\xi_s \tag{2}$$

$$k_s = m_s\omega_s^2 \tag{3}$$

where m_s is the modal mass; c_s is the viscous damping coefficient, which is given by the damping ratio ξ_s; k_s is the stiffness coefficient, which results from the circular frequency ω_s; $\ddot{u}_s(t)$, $\dot{u}_s(t)$, $u_s(t)$ describe the modal acceleration, velocity and displacement, respectively; $f(t)$ is the external excitation force due to ground acceleration. The chosen main structure modal parameters represent typical values of a building that may be susceptible to seismic excitation and therefore may require a mass damper (Table 1). Notice that the choice of structural modal parameters does not influence the outcome of the comparative study under consideration; however, the selection of the modal parameters influences the optimum mass damper parameters that are given for all considered mass damper topologies.

Table 1 Modal parameters of the main structure.

Modal Mass $m_s(kg)$	Damping Ratio ξ_s	Damping Coefficient $c_s(kN \cdot s/m)$	Stiffness Coefficient $k_s(kN/m)$	Frequency (Hz)
150000	2%	67.53	19000	1.79

2.2 Main Structure with a TMD

The model of the main structure with a TMD is given by the following two degrees of freedom system (Fig. 1):

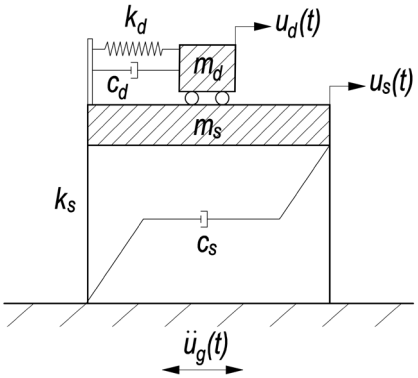

Fig. 1 Analytical model of an SDOF structure with a TMD.

$$\begin{bmatrix} m_s & 0 \\ 0 & m_d \end{bmatrix} \begin{Bmatrix} \ddot{u}_s(t) \\ \ddot{u}_d(t) \end{Bmatrix} + \begin{bmatrix} c_s + c_d & -c_d \\ -c_d & c_d \end{bmatrix} \begin{Bmatrix} \dot{u}_s(t) \\ \dot{u}_d(t) \end{Bmatrix} + \begin{bmatrix} k_s + k_d & -k_d \\ -k_d & k_d \end{bmatrix} \begin{Bmatrix} u_s(t) \\ u_d(t) \end{Bmatrix} = -\begin{bmatrix} m_s \\ m_d \end{bmatrix} \ddot{u}_g(t) \quad (4)$$

where m_d denotes the TMD mass that is determined by the selected mass ratio μ as follows:

$$m_d = \mu \times m_s \quad (5)$$

c_d and k_d are the damping coefficient and stiffness of the TMD, respectively. The parameters of the considered TMD that are numerically optimized for minimum structural displacement. The optimization criterion for minimum structural displacement was chosen to ensure a fair comparison with the performance of the TMDI, which are intended to yield at least a structural displacement response close to its minimum.

2.3 Main Structure with a TMDI with Grounded Inerter

The model of the main structure with a TMDI is given by the following two degrees of freedom system (Fig. 2):

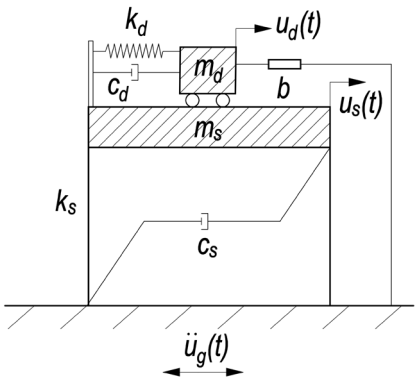

Fig. 2 Analytical model of structure-TMDI system with the inerter connected to the ground.

$$\begin{bmatrix} m_s & 0 \\ 0 & m_d + b \end{bmatrix} \begin{Bmatrix} \ddot{u}_s(t) \\ \ddot{u}_d(t) \end{Bmatrix} + \begin{bmatrix} c_s + c_d & -c_d \\ -c_d & c_d \end{bmatrix} \begin{Bmatrix} \dot{u}_s(t) \\ \dot{u}_d(t) \end{Bmatrix} + \begin{bmatrix} k_s + k_d & -k_d \\ -k_d & k_d \end{bmatrix} \begin{Bmatrix} u_s(t) \\ u_d(t) \end{Bmatrix} = \begin{bmatrix} -m_s \\ -m_d \end{bmatrix} \ddot{u}_g(t) \quad (6)$$

where b denotes the "inertance" with unit (*kg*) that is determined by the selected inertance ratio β as follows:

$$b = \beta \times m_s \quad (7)$$

The inerter force f_b is in proportion to the relative acceleration of the inerter grounds, which is here the difference between ground acceleration $\ddot{u}_g$ and absolute acceleration $\ddot{u}_d + \ddot{u}_g$ of the TMDI mass m_d, and is shown in the following equation. To standardize the subsequent solution, some notations are introduced, as listed in Table 2.

$$f_b = b\ddot{u}_d \quad (8)$$

Table 2 Notations.

Notation	Definition
$\omega_s = \sqrt{k_s/m_s}$	Frequency of the main structure
$\omega_d = \sqrt{k_d/m_d}$	Frequency of the TMDI
$\xi_s = c_s/(2m_s\omega_s)$	Damping ratio of the main structure
$\xi_d = c_d/(2m_d\omega_d)$	Damping ratio of the TMDI
$\nu = \omega_d/\omega_s$	Frequency ratio of the TMDI to the main structure
$\lambda = \omega/\omega_s$	Frequency ratio of excitation to the main structure

The Fourier transforms of the story displacement can be expressed as follows:

$$X(\omega) = [-\omega^2 M + i\omega C + K]^{-1} E f(\omega) \quad (9)$$

$$x_s(\omega) = DX(\omega) = [1 \quad 0]X(\omega) = H_s(\omega) f(\omega) \quad (10)$$

where

$$H_s(\omega) = \frac{(m_s b + m_s m_d)\omega^2 - i\omega(m_s c_d + m_d c_d) - m_s k_d - m_d k_d}{(-\omega^2 m_s + i\omega c_s + i\omega c_d + k_s + k_d)(-\omega^2 m_d - \omega^2 b + i\omega c_d + k_d) - (i\omega c_d + k_d)^2} = \frac{\Delta_1}{\Delta_2} \quad (11)$$

$$\Delta_1 = (m_s b + m_s m_d)\omega^2 - i\omega(m_s c_d + m_d c_d) - m_s k_d - m_d k_d$$

$$\Delta_2 = (m_s b + m_s m_d)\omega^4 - i\omega^3(bc_d + bc_s + m_d c_d + m_d c_s + m_s c_d) - \omega^2(c_d c_s + bk_d + bk_s + m_d k_d + m_d k_s + m_s k_d) + i\omega(c_s k_d + c_d k_s) + k_d k_s \quad (12)$$

To simplify the design procedure, it is assumed that the input of the earthquake is a white noise with zero-mean, that is, $f(\omega) = S_0 = Const.$ Eq. (10) can thus be written as:

$$x_s(\omega) = H_s(\omega)S_0 \tag{13}$$

Define the performance index J as:

$$J = \int_{-\infty}^{+\infty} \|x_s(\omega)\|^2 d\omega = \int_{-\infty}^{+\infty} \|H_s(\omega)\|^2 S_0 d\omega \tag{14}$$

The performance index J can be expressed in terms of the design parameters as:

$$J = \pi S_0 \frac{\beta^2 C_1 + \mu^2 C_2 + 2\beta\mu C_3}{2\mu(\beta+\mu)^2 \nu \omega_s^3 \xi_d} \tag{15}$$

where

$$C_1 = 1 + \mu(1+\mu)\nu^2[-1 + \mu + \mu(1+\mu)\nu^2]$$

$$C_2 = 1 + (1+\mu)^4\nu^4 + (1+\mu)^2\nu^2[-2 + \mu + 4(1+\mu)\xi_d^2]$$

$$C_3 = 1 + \mu(1+\mu)^3\nu^4 + \nu^2[-1 - 2\mu + \mu^3 + 2\mu(1+\mu)^2\xi_d^2]$$

Assuming constant mass and inertance ratios (μ and β), the variance J of Eq. (15) is minimized with respect to the TMDI frequency ratio ν and damping ratio ξ_d by enforcing the following two conditions

$$\frac{\partial J}{\partial v} = 0, \qquad \frac{\partial J}{\partial \xi_d} = 0 \tag{16}$$

These conditions yield a system of two equations from which the optimal tuning parameters ν and ξ_d of the proposed TMDI configuration are found in terms of μ and β as

$$v_{opt} = \frac{\sqrt{(\beta+\mu)[(\beta+\mu)(1-\mu)+2]}}{(1+\beta+\mu)\sqrt{2\mu(1+\mu)}} \tag{17}$$

and

$$\xi_{d,opt} = \frac{(\beta+\mu)\sqrt{\beta(3-\mu)+(4-\mu)(1+\mu)}}{2\sqrt{2\mu(1+\beta+\mu)[\beta(1-\mu)+(2-\mu)(1+\mu)]}} \tag{18}$$

Further, by substitution of the above optimal TMDI tuning parameters into Eq. (15)

the following expression for the achieved minimum variance of performance index J can be obtained.

$$J = \pi S_0 \frac{(1+\mu)^2\sqrt{\beta(3-\mu)+(4-\mu)(1+\mu)}}{\omega_s^3\sqrt{(1+\mu)(1+\beta+\mu)(\beta+\mu)}} \tag{19}$$

It is important to note that by setting $b = \beta = 0$ in Eqs. (17)-(18), the optimal tuning formulae of the classical TMD which minimize the relative displacement variance of an undamped SDOF main structure subjected to white noise excitation can be retrieved. In Section 3, the vibration suppression efficacy of the typical TMDI configuration is systematically compared against the conventional TMD benchmark ($\beta = 0$) for undamped SDOF structure subjected to white noise base excitation.

2.4 Main Structure with a TMDI-I with Floor-connected Inerter

Although grounding the inerter in conventional TMDI systems is effective, this configuration is often impractical, as real buildings rarely permit a direct roof-to-ground inerter connection. To address this practical constraint, an alternative TMDI configuration, termed “TMDI-I”, is proposed, where the inerter is connected to the floor instead of the ground. This research first investigates the performance of the TMDI system when the inerter is connected to the floor. The model of the main structure with TMDI-I is shown in Fig. 3, and the governing equation is listed below:

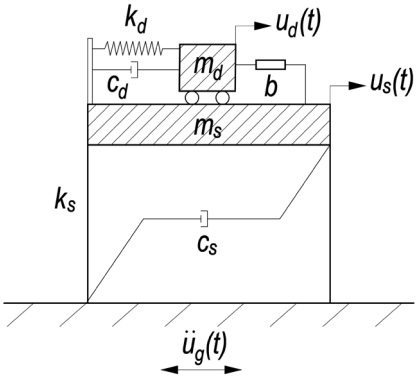

Fig. 3 Analytical model of a SDOF structure with a TMDI-I.

$$\begin{bmatrix} m_s+b & -b \\ -b & m_d+b \end{bmatrix}\begin{Bmatrix} \ddot{u}_s(t) \\ \ddot{u}_d(t) \end{Bmatrix} + \begin{bmatrix} c_s+c_d & -c_d \\ -c_d & c_d \end{bmatrix}\begin{Bmatrix} \dot{u}_s(t) \\ \dot{u}_d(t) \end{Bmatrix} + \begin{bmatrix} k_s+k_d & -k_d \\ -k_d & k_d \end{bmatrix}\begin{Bmatrix} u_s(t) \\ u_d(t) \end{Bmatrix} = -\begin{bmatrix} m_s \\ m_d \end{bmatrix}\ddot{u}_g(t) \tag{20}$$

Note that the inerter force f_b is proprotional to the relative acceleration of the inerter grounds, which is here the difference between main structure modal acceleration $\ddot{u}_s$ and acceleration $\ddot{u}_d$ of the TMDI mass m_d.

$$f_b = b(\ddot{u}_d - \ddot{u}_s) \tag{21}$$

Following similar derivation process, the displacement performance index J assuming white noise excitation can be obtained:

$$J = \pi S_0 \frac{\beta^2 C_1 + \mu^2 C_2 + 2\beta\mu C_3}{2\mu(2\beta+\mu)^2 \nu \omega_s^3 \xi_d} \tag{22}$$

$$C_1 = 1 + \mu[-2 + \mu + 4(1+\mu)(-1+3\mu)\nu^2 + 16\mu(1+\mu)^2\nu^4]$$

$$C_2 = 1 + (1+\mu)^4\nu^4 + (1+\mu)^2\nu^2[-2 + \mu + 4(1+\mu)\xi_d^2]$$

$$C_3 = 1 - \nu^2 + \mu[-1 + 4(1+\mu)^3\nu^4 + \nu^2(-3 + \mu + 3\mu^2 + 8(1+\mu)^2\xi_d^2)]$$

Assuming constant mass ratios μ and β, the performance index J is minimized by solving the differentials of J with respect to frequency ratio ν and damping ratio ξ_d, which yields:

$$\nu_{opt} = \frac{\sqrt{4\beta^2(1-3\mu) + 2\beta(1+3\mu)(1-\mu) + \mu(2-\mu)(1+\mu)}}{\sqrt{2\mu(1+\mu)(1+4\beta+\mu)^2}} \tag{23}$$

and

$$\xi_{d,opt} = \frac{(2\beta+\mu)\sqrt{4\beta^2(5\mu-3) - \beta(4+12\mu-8\mu^2) - \mu(4+3\mu-\mu^2)}}{2\sqrt{2\mu[(\mu-2)\mu(1+\mu)^2 + 16\beta^3(3\mu-1) + 4\beta^2(9\mu^2-2\mu-3) + 2\beta(5\mu^3-\mu^2-7\mu-1)]}} \tag{24}$$

Further, by substitution of the above optimal parameters into Eq. (22), the achieved minimum performance index J can be obtained:

$$J = \pi S_0 \frac{(1+\mu)^2\sqrt{\mu(1+\mu)(4-\mu) + 4\beta^2(3-5\mu) + 4\beta[1-\mu(-3+2\mu)]}}{\omega_s^3(2\beta+\mu)\sqrt{(1+\mu)(1+4\beta+\mu)}} \tag{25}$$

2.5 Main Structure with a TMDI-II with Floor-connected Inerter

An alternative floor-connected inerter configuration is presented in Fig. 4, featuring a parallel inerter-damper assembly arranged in series with a spring. To capture the spring and damper movement separately, an auxiliary degree of freedom in the node between the spring and the viscous damper, $u_b(t)$, is defined. The relevant equations of motion are given below:

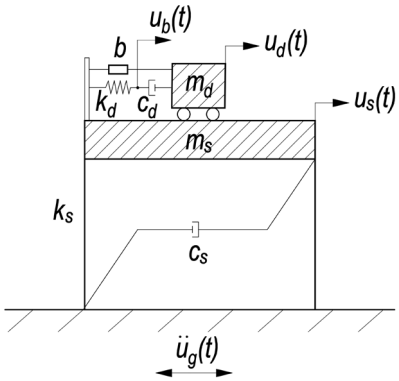

Fig. 4 Mechanical model of a SDOF structure with a TMDI-II.

$$\begin{bmatrix} m_s+b & -b & 0 \\ -b & m_d+b & 0 \\ 0 & 0 & 0 \end{bmatrix} \begin{Bmatrix} \ddot{u}_s(t) \\ \ddot{u}_d(t) \\ \ddot{u}_b(t) \end{Bmatrix} + \begin{bmatrix} c_s & 0 & 0 \\ 0 & c_d & -c_d \\ 0 & -c_d & c_d \end{bmatrix} \begin{Bmatrix} \dot{u}_s(t) \\ \dot{u}_d(t) \\ \dot{u}_b(t) \end{Bmatrix} + \begin{bmatrix} k_s+k_d & 0 & -k_d \\ 0 & 0 & 0 \\ -k_d & 0 & k_d \end{bmatrix} \begin{Bmatrix} u_s(t) \\ u_d(t) \\ u_b(t) \end{Bmatrix} = \begin{bmatrix} -m_s \\ -m_d \\ 0 \end{bmatrix} \ddot{u}_g \tag{26}$$

The previous method of direct derivation of the performance index J from the integral formula is suitable for second-order matrices; with the appearance of third-order matrices in this section, this method is no longer easily applicable. To perform the optimization of the system, the fixed-point method proposed by Den Hartog (1947) is adopted. In the method, the transfer function of the main structure has two invariant points, P and Q, whose positions are independent of ξ_d but functions of λ. The coordinates of P and Q can be obtained by substituting $\xi_d = 0$ and $\xi_d = \infty$. The transfer function can be expressed as:

$$|H(i\omega)| = \sqrt{\frac{A^2 + \xi_d^2 B^2}{C^2 + \xi_d^2 D^2}} \tag{27}$$

where

$$A = -(s^3\beta + s\beta v^2\omega_s^2 + s\mu v^2\omega_s^2 + s\beta\mu v^2\omega_s^2)$$

$$B = -2(\mu v^3\omega_s^3 + \mu^2 v^3\omega_s^3)$$

$$C = s^5\beta + s^3\beta\omega_s^2 + s^3\beta v^2\omega_s^2 + s^3\mu v^2\omega_s^2 + s^3\beta\mu v^2\omega_s^2 + s\beta v^2\omega_s^4 + s\mu v^2\omega_s^4$$

$$D = 2(s^2\mu v^3\omega_s^3 + s^2\mu^2 v^3\omega_s^3 + \mu v^3\omega_s^5)$$

If $s = i\lambda\omega_s,\ \lambda = \omega/\omega_s,$

When

$$\xi_d \to 0\ ,\ |H(i\omega)| = \frac{A}{C}\ and\ \xi_d \to \infty\ ,\ |H(i\omega)| = \frac{B}{D} \tag{28}$$

The coordinates of P and Q can be expressed as:

$$\lambda_P = -\sqrt{\frac{\mu v^2}{b}}\ , \qquad \lambda_Q = \sqrt{\frac{\mu v^2}{b}} \tag{29}$$

When $\xi_d = \infty$, we obtain the following:

$$\frac{\mu v^3 + \mu^2 v^3}{\mu v^3 - \lambda_P^2 \mu v^3 - \lambda_P^2 \mu^2 v^3} = \frac{-(\mu v^3 + \mu^2 v^3)}{\mu v^3 - \lambda_Q^2 \mu v^3 - \lambda_Q^2 \mu^2 v^3} \tag{30}$$

By solving Eq. (30), the optimal frequency ratio of TMDI-II can found:

$$v_{opt} = \sqrt{\frac{\beta}{2\mu(\mu+1) - \beta}} \tag{31}$$

To minimize the maximum value of $|H(i\lambda)|$ at an invariant point P or Q, the optimal condition yields the solution given in Eq. (32).

$$\frac{\partial}{\partial \lambda^2}(|H(i\lambda)|^2)|_{\lambda=\lambda_P} = 0\ , \qquad \frac{\partial}{\partial \lambda^2}(|H(i\lambda)|^2)|_{\lambda=\lambda_Q} = 0 \tag{32}$$

From the above Equation, $\xi_{d,P}^2$ and $\xi_{d,Q}^2$ can be obtained. According to the definition of the optimal damping ratio mentioned by Liu and Liu (2005), the square of the TMDI-II optimal damping ratio is the average of $\xi_{d,P}^2$ and $\xi_{d,Q}^2$, expressed as:

$$\xi_{d,opt}^2 = \frac{\xi_{d,P}^2 + \xi_{d,Q}^2}{2} \tag{33}$$

The optimal damping ratio of TMDI-II can be obtained, as shown below:

$$\xi_{d,opt} = \sqrt{\frac{D_1 + D_2 + D_3 + D_4 - D_5 - 32\mu^7(1+\mu)^5(2+\mu) - 32\beta\mu^5(1+\mu)^4(2\mu^3 - 1 - 7\mu)}{8\beta\mu(1+\mu)^3[\beta - 4\mu(1+\mu)][\beta - 2\mu(1+\mu)]^3}} \tag{34}$$

Where

$$D_1 = 8\beta^2\mu^4(1+\mu)^3(42\mu^2 + 28\mu^3 - 1 - 10\mu)$$

$$D_2 = 8\beta^3\mu^3(1+\mu)^2(4\mu^4 - 42\mu^2 - 17\mu^3 - 4 - 10\mu)$$

$$D_3 = 2\beta^5\mu(4 + 11\mu + 12\mu^2 + 15\mu^3 + 8\mu^4)$$

$$D_4 = 2\beta^4\mu^2(4 + 10\mu + 37\mu^2 + 21\mu^3 - 30\mu^4 - 20\mu^5)$$

$$D_5 = \beta^6(2 + 3\mu + 3\mu^2 + 2\mu^3)$$

3. Structural Responses in the Frequency Domain and Time Domain

3.1 Frequency Domain Analysis

A comprehensive frequency domain analysis of the system is conducted to evaluate the performance of various configurations, including the uncontrolled system, the TMD, conventional TMDI, and the two different TMDI configurations. Fig. 5 shows the frequency transfer function of a SDOF structure under different mass ratio (μ) and inertance ratio (β). The results reveal that TMDIs generally exhibit better vibration control performance compared to the uncontrolled system and the TMD. Notably, conventional TMDI generally achieves the best resonant peak reduction in most of the mass and inertance ratios considered. For instance, at μ = 1% and β = 1%, TMDI reduces the resonant peak by a substantial margin than the floor-connected TMDI configurations (TMDI-I and TMDI-II). However, as the inertance ratio is significantly reduced (e.g., β = 0.01%), the three TMDIs exhibit similar performance.

When μ is held constant, e.g. at 1%, as can be seen from Fig. 5(a)-(c), increasing inertance ratio β generally improves the TMDI performance, but has limited effect on TMDI-I and TMDI-II. For example, at a fixed μ of 1%, reducing β from 1% to 0.01% results in a broader attenuation bandwidth for TMDI-I and TMDI-II. This could be attributed to the enlarged inertance force from the larger relative acceleration between the two terminals of the grounded inerter. On the contrary, the TMDI-I and TMDI-II, due to the fact that the inerter is connected to the floor, the relative acceleration between the two terminals of the floored inerter is smaller, leading to smaller inertance force acting on the main structure.

When β is held constant, e.g. at 1%, as can be seen from Fig. 5(a)(d)(e), increasing the mass ratio μ generally leads to improved peak suppression. This is because a higher mass ratio implies a larger additional mass, which enhances the energy dissipation capability of the TMDI system. It should be noted that all TMDIs shift to a lower frequency range when the mass ratio is increased from 1% to 5%. The frequency range TMDI<TMD<TMDI-I<TMDI-II when μ = 5%. The move of the frequency with the change of mass ratio requires further investigation.

When both mass and inertance ratios increase to 5% (Fig. 5(f)), TMDI continues to exhibit improved performance, while TMDI-I and TMDI-II shows reduced performance. From the observation, there seems to exist an optimal range of mass and intertance ratios for TMDI-I and TMDI-II in terms of performance improvement, however, the TMDI's performance increases with increasing mass and inertance ratios.

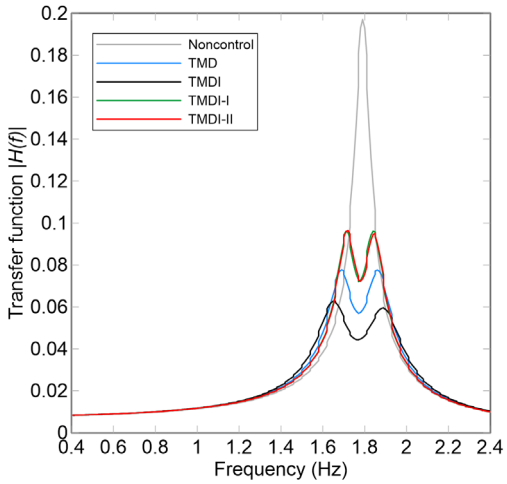

(a) $\mu = 1\%, \beta = 1\%$

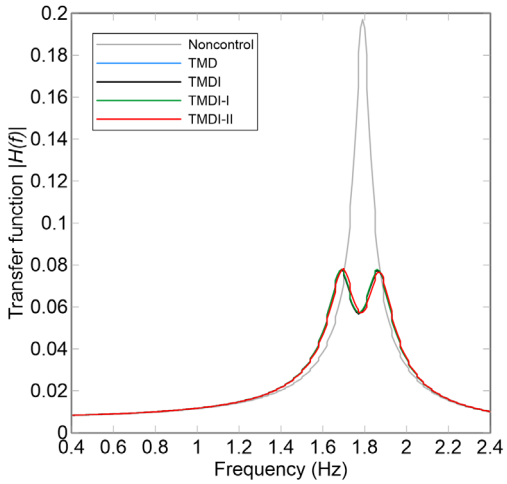

(b) $\mu = 1\%, \beta = 0.01\%$

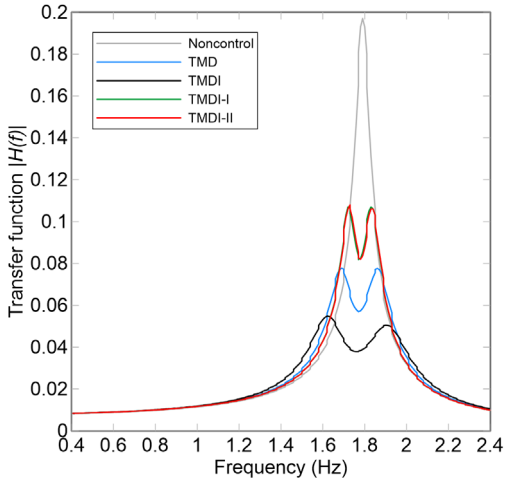

(c) $\mu = 1\%, \beta = 2\%$

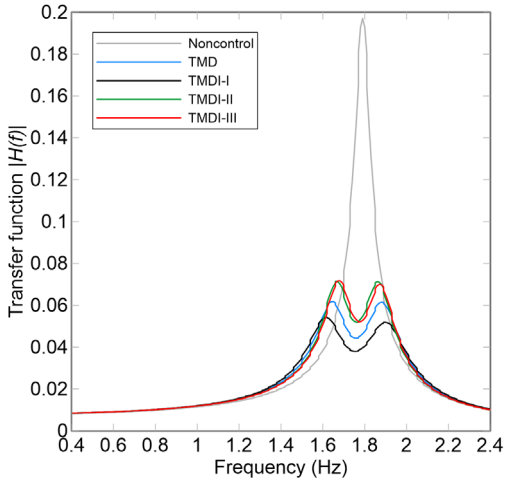

(d) $\mu = 2\%, \beta = 1\%$

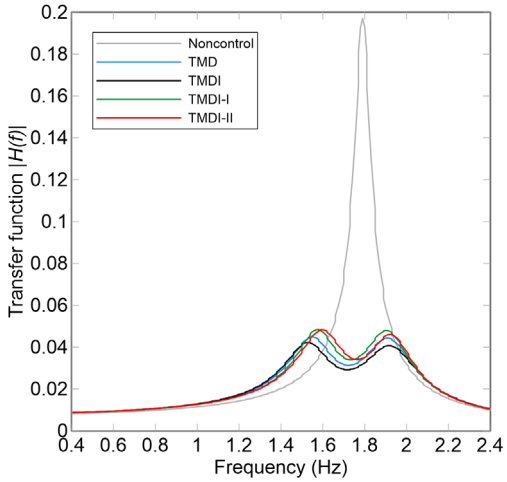

(e) $\mu = 5\%, \beta = 1\%$

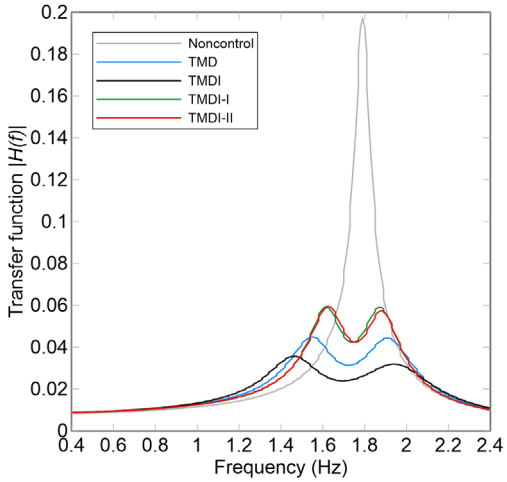

(f) $\mu = 5\%, \beta = 5\%$

Fig. 5 Displacement transfer function curves of the systems.

3.2 Time History Analysis

To further investigate the characteristics of the proposed TMDI configurations, time histories analysis of a SDOF structure with different damper systems but with the same mass ratio (1%) and two designated inertance ratios (1% and 0.01%) were conducted. Two earthquakes, namely an artificial earthquake generated from a white noise spectrum and the 1952 Taft earthquake were used as the ground excitations. The parameters of the main structure are listed in Table 1.

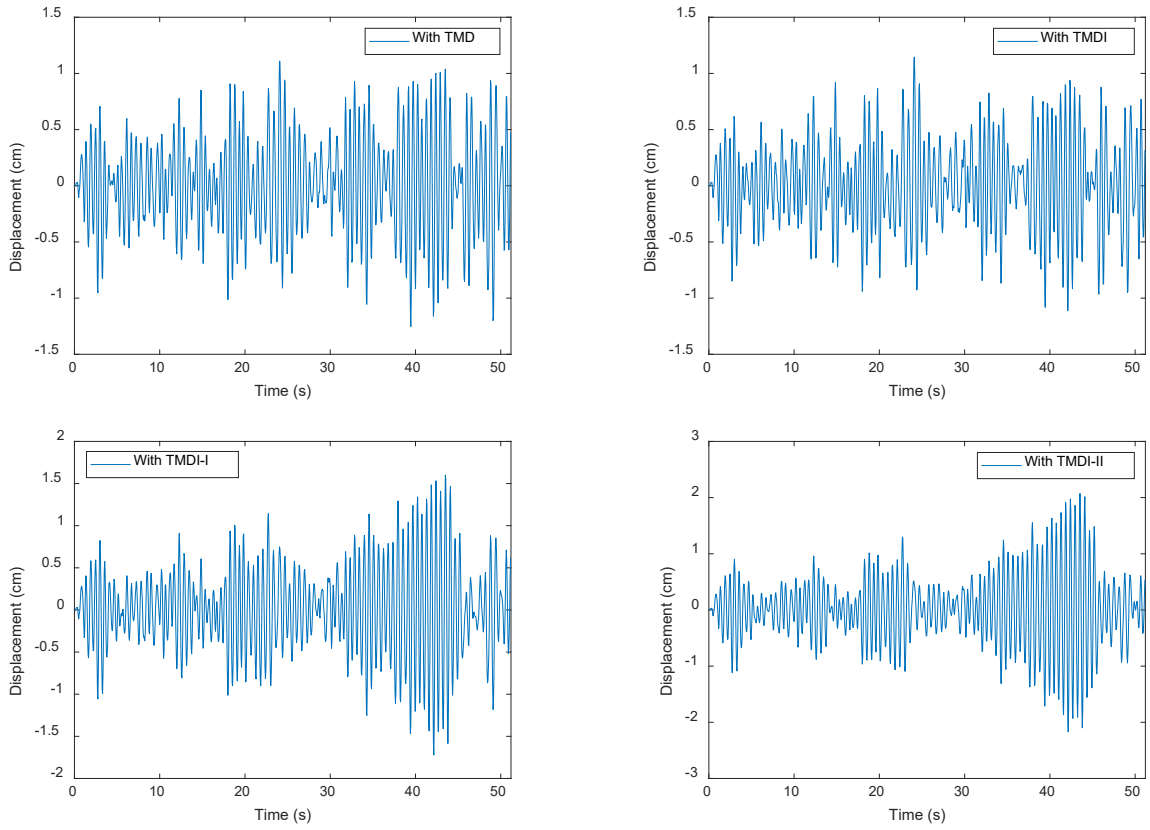

Fig. 6 Displacement time histories under white noise input $(\mu = 1\%, \beta = 1\%)$.

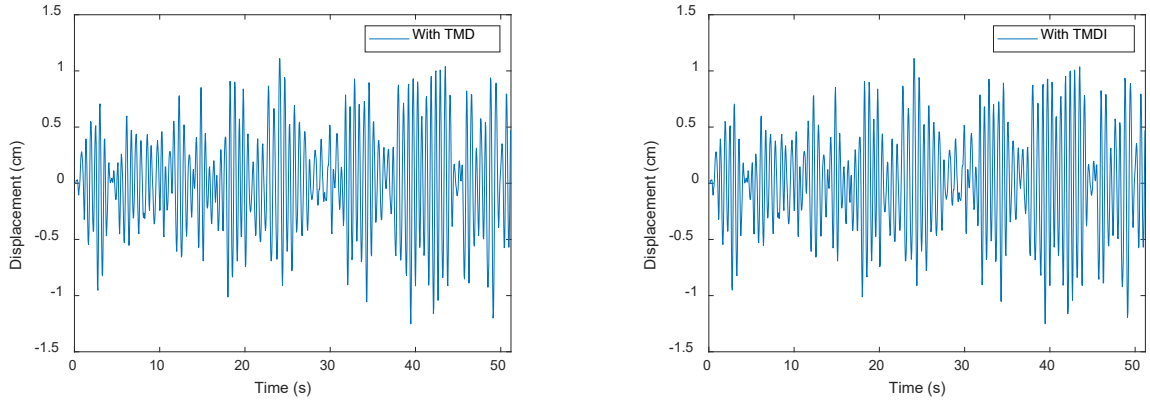

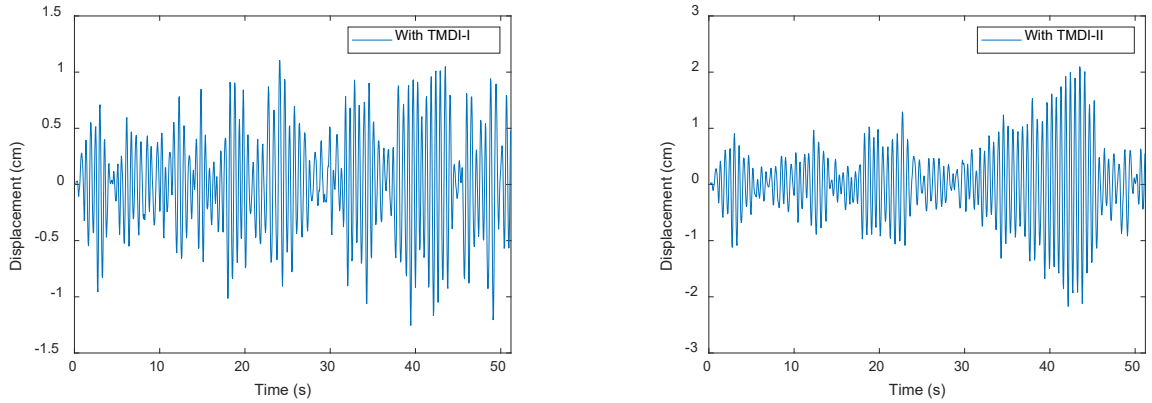

Fig. 7 Displacement time histories under white noise input $(\mu = 1\%, \beta = 0.01\%)$.

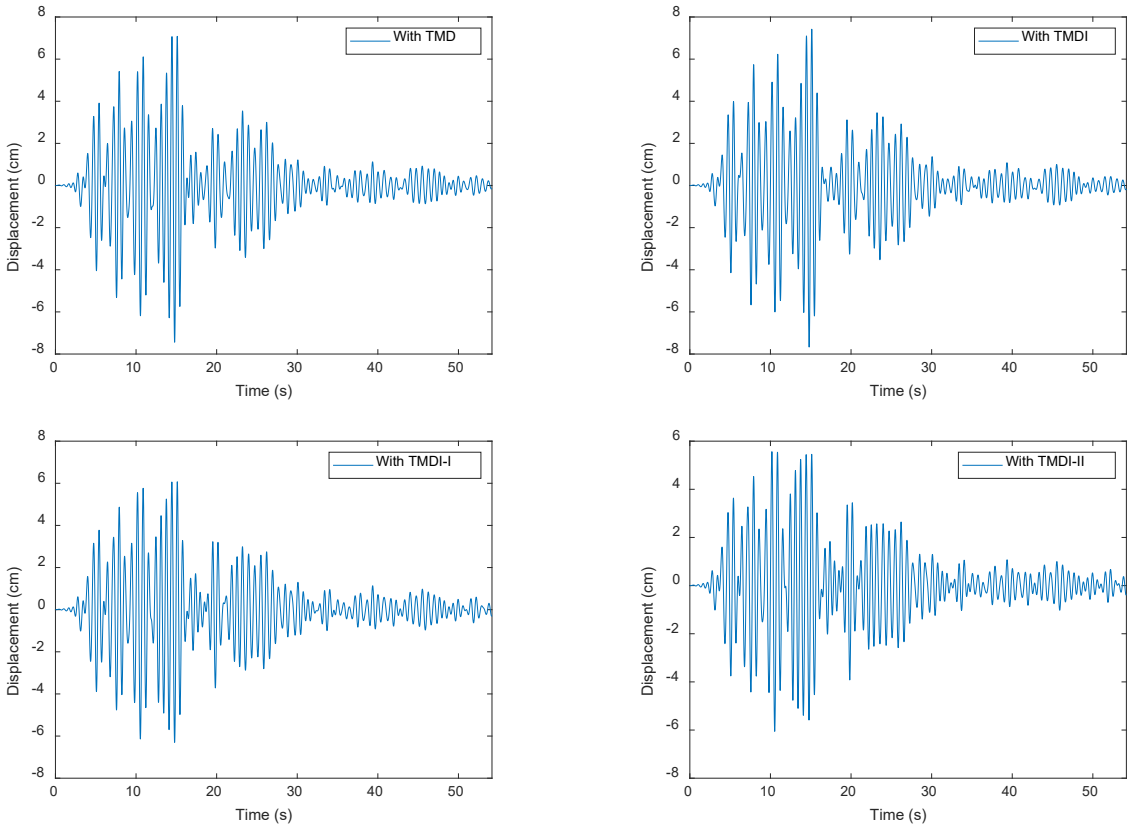

Fig. 8 Displacement time histories under 1952 Taft acceleration input $(\mu = 1\%, \beta = 1\%)$.

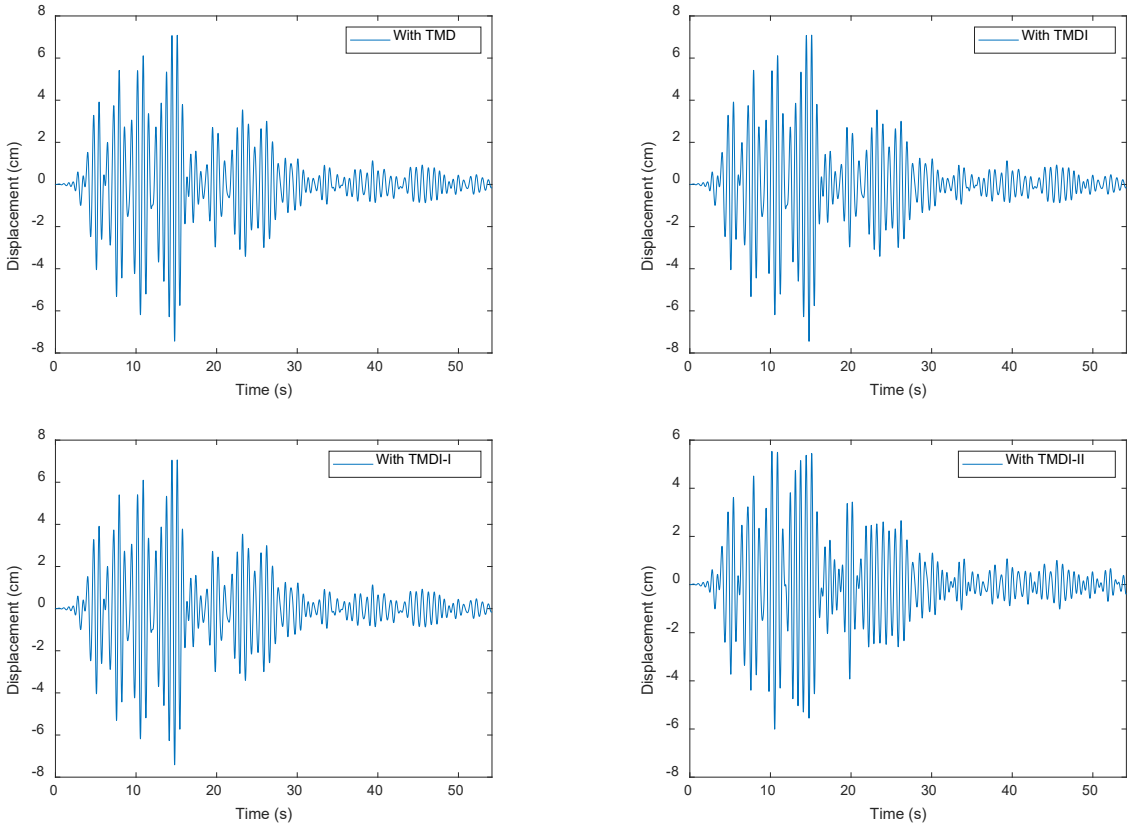

Fig. 9 Displacement time histories under 1952 Taft acceleration input $(\mu = 1\%, \beta = 0.01\%)$.

Table 3 Displacement response of the SDOF structure with different damper configurations excited by ground motion.

Parameter	Displacement response	White noise				Taft			
		TMD	TMDI	TMDI-I	TMDI-II	TMD	TMDI	TMDI-I	TMDI-II
$\mu = 1\%$, $\beta = 1\%$	Peak displacement (cm)	1.2524	1.1459	1.7213	2.1739	7.4396	7.6693	6.3008	6.0548
	RMS displacement (cm)	0.4363	0.3924	0.5267	0.6273	1.6487	1.6738	1.5863	1.5468
$\mu = 1\%$, $\beta = 0.01\%$	Peak displacement (cm)	1.2524	1.2498	1.2543	2.1698	7.4396	7.4469	7.4149	6.0074
	RMS displacement (cm)	0.4363	0.4356	0.4371	0.6269	1.6487	1.6491	1.6467	1.5377

Fig. 6 to 9 illustrates the displacement responses of the structure with different damper configurations. As shown in Fig. 6 and Table 3, the floor-connected TMDIs (TMDI-I and TMDI-II) exhibit higher story displacement than that of the TMD and TMDI for the white noise input. Specifically, when $\mu = 1\%$ and $\beta = 1\%$, TMDI-II displays the largest peak displacement (2.1739 cm) and root-mean-square (RMS) displacement (0.6273 cm) among all configurations. When $\mu = 1\%$ and $\beta = 0.01\%$, both TMDI and TMDI-I configurations effectively degenerate into a TMD-like system, resulting in very similar displacement responses to the standalone TMD. In contrast, the TMDI-II system exhibits a significantly higher displacement response under white noise ground excitation, reaching a peak displacement of 2.1698 cm, which is substantially larger than the other configurations. This indicates that TMDI-II is less effective in mitigating vibrations under white noise excitation.

However, it is not the case for the Taft excitation shown in Fig. 7 and Table 3. Fig. 7 and Table 3 show that when $\mu = 1\%$ and $\beta = 1\%$, the peak displacement responses of the main structure with TMDI-II exhibits the best performance with the lowest peak displacement (6.0548 cm) and RMS displacement (1.5468 cm), followed by TMDI- I (6.3008 cm peak displacement), and TMD (7.4396 cm peak displacement), and all of them perform better the TMDI (7.6693 cm peak displacement). When $\mu = 1\%$ and $\beta = 0.01\%$, the performance trends remain consistent. TMDI and TMDI-I degenerate into the TMD system, and the displacement responses are similar, while TMDI-II continues to show the best performance with the lowest peak displacement (6.0074 cm) and RMS displacement (1.5377 cm). This indicates that even at very low inertance ratios, the TMDI-II configuration maintains its superior vibration mitigation capability under Taft wave excitation, outperforming all other configurations. Overall, the conventional TMDI with grounded inerter shows distinct better performance under white noise ground excitation, while TMDI-II system shows slightly better performance under Taft wave excitation.

4. CONCLUSIONS

In this paper, two novel floor-connected TMDI configurations are introduced. Through analytical modeling, frequency domain analysis, and time history simulations, and the following conclusions are drawn:

(1) The strategic positioning of the inerter significantly influences vibration attenuation efficiency. The conventional grounded TMDI demonstrates superior vibration suppression capability compared to the TMD. The series floor-connected TMDI (TMDI-II) outperforms the parallel floor-connected configuration (TMDI-I), which exhibits the lowest performance among the evaluated systems. Grounded configurations consistently outperform floor-connected counterparts due to enhanced energy dissipation pathways.

(2) Analytical derivation using integral formulas and fixed-point theory establishes closed-form solutions for optimal frequency ratio and damping ratio in SDOF systems. These key parameters provide critical design guidelines for achieving maximum vibration reduction.

(3) Time history simulations under white noise and Taft wave excitations confirm the performance hierarchy. Peak displacement responses follow TMDI-II < TMDI-I <

TMD < TMDI sequence under Taft wave excitation. At small inertance ratio $\beta = 0.01\%$, TMDI and TMDI-I configurations degenerate to TMD-equivalent behavior.

In this paper, only single-degree-of-freedom structures with a TMDI are discussed, and the type and number of ground motions used are limited. The response of the multi-degree-of-freedom structure with a TMDI and different ground motion inputs will be further investigated in detail in the future.

REFERENCES

Dai, J., Xu, Z. D., Gai, P. P., and Hu, Z. W. (2021). Optimal design of tuned mass damper inerter with a Maxwell element for mitigating the vortex-induced vibration in bridges. *Mechanical Systems and Signal Processing,* 148, 107180.

De Domenico, D., Ricciardi, G., and Benzoni, G. (2018). Analytical and finite element investigation on the thermo-mechanical coupled response of friction isolators under bidirectional excitation. *Soil Dynamics and Earthquake Engineering*, 106, 131–147.

Den Hartog, J. P. (1947). *Mechanical vibrations*. McGraw-Hill Book Company, Inc., New York, NY.

Giaralis, A., and Petrini, F. (2017). Wind-induced vibration mitigation in tall buildings using the tuned mass-damper-inerter. *Journal of Structural Engineering,* 143(9), 04017127.

Giaralis, A. and Taflanidis, A. A. (2018). Optimal tuned mass-damper-inerter (TMDI) design for seismically excited MDOF structures with model uncertainties based on reliability criteria. *Structural Control & Health Monitoring*, 25(2), e2082.

Khorsand, S. and Rofooei, F. R. (2024). H∞ optimum design and nonlinear seismic performance assessment of tuned-mass-damper-inerter (TMDI) supported by an auxiliary structure. *Structures*, 69, 107257.

Lara-Valencia, LA., Farbiarz-Farbiarz, Y. and Valencia-González, Y. (2020). Design of a tuned mass damper inerter (TMDI) based on an exhaustive search. *Shock and Vibration*, 210, 8875268.

Lazar, I. F., Neild, S. A. and Wagg, D. J. (2014). Using an inerter-based device for structural vibration suppression. *Earthquake Engineering & Structural Dynamics*, 43(8), 1129–1147.

Liu, K. and Liu, J. (2005). The damped dynamic vibration absorbers: revisited and new result. *Journal of Sound and Vibration*, 284(3-5), 1181–1189.

Li, W. J. (2022). *Research on constrained multi-objective optimization theory and its application in wind-induced vibration control of super high-rise buildings*. Doctoral dissertation. Shantou University.

Marian, L. and Giaralis, A. (2014). Optimal design of a novel tuned mass-damper-inerter (TMDI) passive vibration control configuration for stochastically support-excited structural systems. *Probabilistic Engineering Mechanics*, 38, 156–164.

Petrini, F., Giaralis, A., and Wang, Z. X. (2020). Optimal tuned mass-damper-inerter (TMDI) design in wind-excited tall buildings for occupants' comfort serviceability performance and energy harvesting. *Engineering Structures,* 204, 109904.

Pietrosanti, D., De Angelis, M. and Basili, M. (2017). Optimal design and performance evaluation of systems with Tuned Mass Damper Inerter (TMDI). *Earthquake Engineering & Structural Dynamics*, 46(8), 1367–1388.

Pietrosanti, D., De Angelis, M. and Basili, M. (2020). A generalized 2-DOF model for optimal design of MDOF structures controlled by Tuned Mass Damper Inerter (TMDI). *International Journal of Mechanical Sciences*, 185, 105849.

Ruiz, R., Taflanidis, A. A., Giaralis, A. and Lopez-Garcia, D. (2018). Risk-informed optimization of the tuned mass-damper-inerter (TMDI) for the seismic protection of multi-storey building structures. *Engineering Structures*, 177, 836-850.

Smith, M. C. (2002). Synthesis of mechanical networks: The inerter. *IEEE Transactions on Automatic Control*, 47(10), 1648–1662.

Song, G., Ma, N., and Li, H. N. (2006). Applications of shape memory alloys in civil structures. *Engineering Structures,* 28(9), 1266–1274.

Sun, D. C., and Tong, L. Y. (2004). A compressional-shear model for vibration control of beams with active constrained layer damping. *International Journal of Mechanical Sciences,* 46(9), 1307–1325.

Zhang, Z. L., Chen, B. and Hua, X. G. (2023). Closed-form optimization of tuned mass-damper-inerter (TMDI) in flexible structures. *Journal of Building Engineering*, 72, 106554.

Zhang, Z. L., and Fitzgerald, B. (2020). Tuned mass-damper-inerter (TMDI) for suppressing edgewise vibrations of wind turbine blades. *Engineering Structures,* 221, 110928.